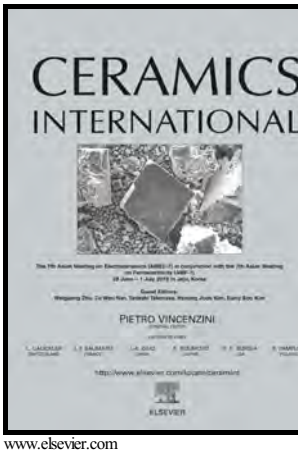

Structure and microwave dielectric properties of $(1–x)Nd(Zn_{0.5}Ti_{0.5})O_3$-$xCa_{0.61}Nd_{0.26}TiO_3$ ceramics

Jiamao Li, Chuangang Fan, Songlin Ran

PII: S0272-8842(15)01680-6
DOI: http://dx.doi.org/10.1016/j.ceramint.2015.08.154
Reference: CERI11251

To appear in: *Ceramics International*

Received date: 7 August 2015
Revised date: 26 August 2015
Accepted date: 27 August 2015

Cite this article as: Jiamao Li, Chuangang Fan and Songlin Ran, Structure and microwave dielectric properties of $(1–x)Nd(Zn_{0.5}Ti_{0.5})O_3$-$xCa_{0.61}Nd_{0.26}TiO$ ceramics, *Ceramics International* http://dx.doi.org/10.1016/j.ceramint.2015.08.154

Structure and microwave dielectric properties of (1-*x*)Nd($Zn_{0.5}Ti_{0.5}$)O_3-*x*$Ca_{0.61}Nd_{0.26}TiO_3$ ceramics

Jiamao Li, Chuangang Fan, Songlin Ran

School of Materials Science and Engineering, Anhui University of Technology, Maanshan 243002, PR China

Abstract: Structure and microwave dielectric properties of (1-*x*)Nd($Zn_{0.5}Ti_{0.5}$)O_3-*x*$Ca_{0.61}Nd_{0.26}TiO_3$ ($0.2 \le x \le 0.8$) ceramics prepared by the conventional solid-state reaction route were investigated in detail. It was found that the crystal structure and microwave dielectric properties depended strongly on $Ca_{0.61}Nd_{0.26}TiO_3$ content. In the whole investigated compositional range, the complete solid solutions with perovskite structure were formed together with a small amount of Zn_2TiO_4 secondary phase. However, a phase transformation from monoclinic to orthorhombic structure was also observed when $x > 0.6$, accompanying with the disappearance of cation ordering. With the increase of $Ca_{0.61}Nd_{0.26}TiO_3$ addition, both the grain size and the dielectric constant (ε_r) increased. The quality factor ($Q \times f$) was closely related to the grain size and cation ordering of the ceramics. The drastic drop in the temperature coefficient of resonant frequency (τ_f) might be attributed to the elimination of cation ordering. After being sintered at 1375 °C for 4 h, 0.4Nd($Zn_{0.5}Ti_{0.5}$)O_3-0.6$Ca_{0.61}Nd_{0.26}TiO_3$ exhibited high density, uniform microstructure and excellent microwave dielectric properties of ε_r = 56.3, $Q \times f$ = 54400 GHz and τ_f = +0.3 ppm/°C.

Key words: Nd($Zn_{0.5}Ti_{0.5}$)O_3; $Ca_{0.61}Nd_{0.26}TiO_3$; Perovskite; Structure; Microwave dielectric properties

* Corresponding author. Tel. & fax: +86 555 2311570.

E-mail address: agdjiamaolee@126.com (J.M. Li).

1. Introduction

With the rapid progress of the wireless communication including mobile phone, GPS, DBS TV and so on, the demand on new material systems with combined dielectric properties has been increasing [1, 2]. As microwave components such as resonators and filters applied to the wireless communication, microwave dielectric ceramics should possess three critical characteristics of a high dielectric constant (ε_r) to reduce the size of devices, a high quality factor ($Q \times f$) for achieving prominent frequency selectivity and stability and a near-zero temperature coefficient of resonant frequency (τ_f) for temperature stability [3, 4]. However, it is difficult for some single compounds to achieve these demands mentioned above simultaneously, espcially a near-zero τ_f. Therefore, some measures have to be taken to obtain a nero-zero τ_f. Usually, combining two or more compounds with similar crystal structure and different microwave dielectric properties to form a solid solution or mixed phases is an effective and promising approach to reach this target. For example, the solid solutions $0.7Ba(Co_{1/3}Nb_{2/3})O_3$–$0.3Ba(Ni_{1/3}Nb_{2/3})O_3$ and $0.7Ba(Co_{1/3}Nb_{2/3})O_3$–$0.3Ba(Zn_{1/3}Nb_{2/3})O_3$ with the complex perovskite structure separately obtained by cation substitution show the zero τ_f since $Ba(Ni_{1/3}Nb_{2/3})O_3$ and $Ba(Zn_{1/3}Nb_{2/3})O_3$ ceramics have the negative τ_f whereas $Ba(Co_{1/3}Nb_{2/3})O_3$ has the positive τ_f [5, 6].

In recent years, many efforts have been made to investigate $Ln(B_{0.5}Ti_{0.5})O_3$ (Ln = La, Sm, Nd, Dy, Y; B =Mg, Zn, Co) ceramics with complex perovskite structure due to their excellent microwave dielectric properties, especially ultrahigh quality factor [7-10]. These investigations have shown that the B-site cations and their ordering have significant effects on the crystal symmetry and subsequently the microwave dielectric properties. According to a previous report, $Nd(Zn_{0.5}Ti_{0.5})O_3$ (hereafter referred to as NZT) performs a moderate dielectric constant (ε_r ~31.6),

an ultrahigh value $Q\times f$ value (170,000 GHz) but relative large negative τ_f (~ -42 ppm/°C) [8]. Clearly, the key issue which limits the practical application of NZT is a relatively large temperature coefficient of resonant frequency. Nevertheless, unlike the Ba-based complex perovskite ceramics, the τ_f of NZT ceramics can not be adjusted to zero by individually substituting Mg^{2+} and Co^{2+} cations for Zn^{2+} cation because they have similar negative τ_f [11-13]. Therefore, to tune the τ_f to zero, introducing some compounds with the different crystal structure and positive τ_f to NZT ceramics should be a more effective method. Related investigations have shown that moderate ε_r, high $Q\times f$ value and near zero τ_f have been achieved in some new ceramic systems such as NZT-$SrTiO_3$ (ε_r = 54.2, $Q\times f$ = 84000 GHz, τ_f = 0 ppm/°C) and NZT-$CaTiO_3$ (ε_r = 45, $Q\times f$ = 56000 GHz, τ_f = 0 ppm/°C) [15, 16].

$Ca_{0.61}Nd_{0.26}TiO_3$ (hereafter referred to as CNT) ceramics was reported to be a good dielectric resonator material with an ε_r value of ~108, a $Q\times f$ value of 17200 GHz, and a τ_f value of ~270 ppm/°C [17] and has been proved to be a suitable compound to compensate the negative τ_f value of dielectric ceramics, producing efficient ceramics with temperature stability at resonant frequency in many studies [18-21].

In a precious work, NZT was added to CNT to create a ceramic system of $(1-x)$CNT–xNZT (x = 0.00–0.40) [22]. Unfortunately, the new ceramic system with a near-zero τ_f was not obtained although high ε_r and high $Q\times f$ value (ε_r = 78.8, $Q\times f$ =19200 GHz, τ_f = +135 ppm/°C for x = 0.15; ε_r = 71.8, $Q\times f$ =17300 GHz, τ_f = +94 ppm/°C for x = 0.20) was achieved, indicating these materials can not be used for practical applications in communication components such as filters and antennas. In the present study, we combined NZT with CNT by forming the (1-x)NZT-xCNT ($0.2 \le x \le 0.8$) ceramic system and managed to obtain a new dielectric material system with a

near-zero τ_f. The crystal structure, microstructure and microwave dielectric properties of the resulting (1-*x*)NZT-*x*CNT ($0.2 \leq x \leq 0.8$) ceramic system were examined in detail.

2. Experimental procedure

(1-*x*)NZT-*x*CNT ($0.2 \leq x \leq 0.8$) ceramics were prepared by the conventional solid-state reaction route using high-purity carbonate or oxide powders (>99.9%) of Nd_2O_3, ZnO, $CaCO_3$ and TiO_2 as starting materials. At first, NZT and CNT powder was individually synthesized by mixing the starting materials according to the desired stoichiometry, ball milling in ethanol for 8 h in polyethylene bottles with zirconia balls. After dried at 80 °C for about 6 h, both mixtures were calcined at 1100 °C for 2 h and 3 h, respectively. Subsequently, these calcined powders were mixed according to the composition of (1-*x*)NZT-*x*CNT (x = 0.2, 0.4, 0.6, 0.8) and remilled 8 h in ethanol. Finally, the fine powders with 8 wt.% PVA solution as a binder were uniaxially pressed under the pressure of 100 MPa, and then cold isostatically pressed into pellets with dimensions of 12 mm diameter and 6 mm thickness under the pressure of 300 MPa. These pellets were muffled by a powder of the same composition and sintered at 1325 -1400 °C for 4 h in air. The muffling was performed to avoid ZnO volatilization at elevated sintering temperatures. After cooling from the sintering temperature to 1000 °C at a rate of 2 °C/min, the ceramics were naturally cooled inside the furnace.

The bulk densities of the sintered pellets were measured with the liquid Archimedes method using distilled water as the liquid. The phase identification was carried out by the X-ray diffraction method using Cu Kα radiation (40kV and 20mA, XRD, D8 Advance, Bruker, Germany). The microstructures of the sintered, polished and thermally etched surfaces were observed by scanning electron microscopy (SEM, JEOL JSM 6490, Japan). The dielectric constant and unloaded *Q*

value at microwave frequencies were measured using the Hakki-Coleman dielectric resonator method, as modified and improved by Courtney [23, 24]. The temperature coefficient of resonant frequency (τ_f) was measured in the temperature range from 25 to 80 °C and the τ_f value was calculated from the following equation:

$$\tau_f = \frac{f_{80} - f_{25}}{f_{25} \bullet 55} \times 10^6 (ppm/^O C) \quad (1)$$

where f_{25} and f_{85} were the resonant frequency at 25 and 80 °C, respectively.

3. Results and discussion

The bulk densities of (1-*x*)NZT-*x*CNT ceramics with different *x* values as a function of sintering temperature are illustrated in Fig. 1. The bulk density of the samples initially increases with the increase of sintering temperature, attaining a maximum value at 1375 °C. This increase in the bulk density can be attributed to the formation of dense microstructures. The bulk density decreases when the sintering temperature exceeds 1375 °C, possibly implying an inhomogeneous microstructure evolution. Moreover, the bulk density of (1−*x*)NZT−*x*CNT ceramics decreases steadily with the *x* value since CNT (4.57 g/cm^3) possesses a lower density than that of NZT (6.94 g/cm^3) [8, 18]. At 1375 °C, the bulk density of the (1−*x*)NZT−*x*CNT ceramics decreases from 6.27 g/cm^3 to 4.87 g/cm^3 as the *x* value increases from 0.2 to 0.8.

Fig. 2 shows the X-ray diffraction patterns of (1-*x*)NZT-*x*CNT ceramics with different *x* values sintered at 1375 °C for 4 h in air. For the entire investigated compositional range, the complete solid solutions with the perovskite structure were formed. It has been reported that CNT has an orthorhombic perovskite structure with four formula units per unit-cell similar to $GdFeO_3$ (JCPDS # 78-0451) and NZT exhibits a perovskite structure with four formula units per unit-cell similar to $Nd(Mg_{0.5}Ti_{0.5})O_3$ (JCPDS # 77-2426), respectively [7, 8, 17, 25]. Therefore, NZT and CNT

possess the similar structure and then can form the complete solid solution. However, two extra weak diffraction peaks corresponding to Zn_2TiO_4 phase at about 2θ = 30.4° and 54.2° were found for the compositions of x = 0.2, 0.4 and 0.6, implying that a small amount of Zn_2TiO_4 secondary phase was formed.

According to the Vegard′s law [26], a linear change of the unit-cell parameters can be expected for the formation of complete solid solutions. Some of the crystallographic data calculated from the XRD diffraction patterns by the least square method are listed in Table 1. The unit cell volume exhibits a quasi-linear dependence decreasing from 237.9 $Å^3$ to 236.95 $Å^3$ with the increasing x value from 0.2 to 0.8 though lattice constants a, b and c vary in different ways. This is due to the fact that the effective average ionic radius of Ti^{4+} (0.605 Å) in CNT is smaller than that of the Zn^{2+} (0.74 Å) on the B-site in NZT at the same coordination number [27]. Meanwhile, with the increasing content of CNT, more vacancies will occupy the A-site in (1-x)NZT-xCNT [22, 25]. As a result, unit cell volume decreases with the increase of CNT content. The XRD results observed by Fig. 2 also present that the diffraction peaks slightly shift to a higher angle with the increasing amount of CNT, which implies that the unit cell volume gradually decreases. The relative densities (shown in Table 1) for all the compositions are higher than 97%, indicating that all the samples are well sintered.

In fact, all diffraction peaks can be indexed according to a simple perovskite structure. A series of extra weak reflections were observed in Fig. 2 for all the investigated samples, indicating that the unit cell was doubled in the perovskite due to the cation ordering and the tilting of oxygen octahedral in the ABO_3 perovskite structure. In perovskite structure, two common mechanisms of cation ordering and tilting of oxygen octahedral are known to the origin of unit cell doubling [28,

29]. According to Glazer′s theory [30, 31], superlattice reflections with specific combinations of odd (*o*) and even (*e*) Miller indices point to definite types of deviation of the structure from the undistorted cubic one, such as octahedral in-phase tilting *(ooe*, *oeo*, *eoo*), anti-phase tilting (*ooo*, h + k + l＞3), chemical ordering (*ooo*) and anti-parallel displacement of A-site cations (*eeo*, *eoe*, *oee*).

In precious investigations, the crystal structures of some analogues to NZT such as $La(Mg_{0.5}Ti_{0.5})O_3$, $La(Mg_{0.5}Sn_{0.5})O_3$ and $La(Zn_{0.5}Ti_{0.5})O_3$ have been reported [32-34]. The structure of $La(Mg_{0.5}Ti_{0.5})O_3$ is a monoclinic ($P2_1/n$, z=4) and is characterized by both in-phase and anti-phase tilting of the oxygen octahedra, La displacement and high degree of Mg/Ti cation ordering. As reported by Fu *et al.* [25], the structure of CNT is an orthorhombic (P*nma*, z=4) and is determined by both in-phase and anti-phase tilting of the oxygen octahedral. From the XRD patterns in Fig. 2, approximate structure changes of (1-*x*)NZT-*x*CNT are suggested and summarized in Table 2. In the entire investigated compositions, in-phase tilting occurring from the (321) plane emerges in the (1-*x*)NZT-*x*CNT system obviously. The evidence of anti-phase tilting owing to the existence of the (331) reflection is also found for all the compositions. These results are good agreement with the theory reported by Reaney *et al*. that the tilting of oxygen octahedral occurs in both in-phase and anti-phase when tolerance factor $t<0.965$ (t of (1-*x*)NZT-*x*CNT shown in Table 2 is 0.921~0.949) [35]. However, it is of interest that 1/2 (111) reflection due to the cation ordering in NZT disappears at $x>0.6$, which implies that cation ordering is disrupted at $x>0.6$. As is well known, the cation ordering in $A^{2+}B^{4+}O_3$ perovskite compounds is very sensitive to the slight variation in composition [36, 37]. For example, the cation disordering in $Ba(Zn_{1/3}Ta_{2/3})O_3$ system will occur even if adding only 5 mol% $BaZrO_3$ or $SrTiO_3$ to

$Ba(Zn_{1/3}Ta_{2/3})O_3$ [36]. However, Table 2 indicates that the B-site ordering of cations in NZT persists up to 60 mol% CNT. This difference may arise from the fact that the solid solution system in this work is not between $A^{2+}B^{4+}O_3$ perovskite compounds but between $A^{3+}B^{3+}O_3$ and $A_{0.87}{}^{2+}B^{4+}O_3$ perovskite compounds. In this case, the charge difference between two B-site cations, which is the main driving force for cation ordering, is maintained. In addition, whether the short-range ordering of cation can exist at $x>0.6$ remains unclear because the XRD method is only sensitive to the long-range ordering of cation and needs to further investigate by using high resolution XRD patterns or neutron diffraction techniques.

Fig. 3 shows the variation of 1/2(200) and 1/2(211) reflections of (1-*x*)NZT-*x*CNT ceramics with the *x* value in more detail. It can be seen that the splitting degree of 1/2(200) and 1/2(211) reflections decreases with the increasing CNT content, showing the structure symmetry of NZT with a space group $P2_1/n$ is lower than that of CNT with a space group P*nma*.

Fig. 4 shows the SEM photographs of polished surface of thermal etched (1−*x*)NZT–*x*CNT ceramics sintered at 1375 °C for 4 h. For all compositions, low level porosity and densed ceramics are obtained. The increasing content of CNT addition leads to promote the grain growth and then the grain size tends to become larger. As the *x* value increases from 0.2 to 0.8, the average grain size increases from ~ 2 μm to ~ 7.4 μm.

The SEM photographs of polished surface of thermal etched (1−*x*)NZT–*x*CNT ceramics sintered at different temperatures for 4 h are illustrated in Fig. 5. As shown in Fig. 5, the porous structure is clearly found in the sample sintered at 1325 °C and the amount of pore decreases as the sintering temperature increases. The densed ceramics are achieved when further raising the sintering temperature and the grain size of all samples increases continuously with the sintering

temperature. For example, the average grain size for the sample sintered at 1350 °C is ~1.8 μm and for the sample at 1400 °C is ~9 μm. As is well known, there is a good relation in increasing of the $Q\times f$ value and grain size. As the grain size increases, the grain boundary area reduces, and thus decreasing the lattice imperfections and dielectric losses. ~~However, over-high sintering temperature (1400 °C) causes the abnormal grain growth and inhomogeneous microstructure, which might deteriorate the microwave dielectric properties.~~

The dielectric constant (ε_r) of (1−*x*)NZT–*x*CNT ceramics with different *x* values as a function of sintering temperature is illustrated in Fig. 6. It can be found that the dielectric constant firstly increases with the increase of sintering temperature due to a denser specimen, then reaching the maximum at 1375 °C, it decreases finally. Therefore, the relationship between ε_r and sintering temperature exhibits the same trend as that between density and sintering temperature since higher density means lower porosity. The ε_r value for 0.4NZT-0.6CNT ceramics varies from 40.6 to 56.3 as the sintering temperature raises from 1325 °C to 1400 °C and a maximum ε_r value of 56.3 was achieved at 1375 °C, indicating that further increase in the sintering temperature does not certainly lead to a higher dielectric constant. In addition, it is well known that dielectric constant varies with the total molecular dielectric polarizability and molar volume according to the Clausius-Mossotti equation. Therefore, the contraction of the unit cell volume displayed in Table 1 will cause the increase of dielectric polarizability in the unit cell volume, and then result in the increase of the dielectric constant. As expected, the ε_r of (1−*x*)NZT–*x*CNT ceramics sintered at 1375 °C increases from 34.1 to 76 as the amount of CNT increases from 0.2 to 0.8.

The quality factor ($Q\times f$) value of (1−*x*)NZT–*x*CNT ceramics with different *x* values sintered at various temperatures for 4 h are demonstrated in Fig. 7. With the increase of sintering temperature,

the $Q\times f$ value increases to a maximum value due to higher density and decreased thereafter owing to the lower density ~~caused by the abnormal grain growth and inhomogeneous microstructure because of an over-high sintering~~. Clearly, the variation in the $Q\times f$ value of $(1-x)$NZT–xCNT ceramics is good agreement with that of density, suggesting that the $Q\times f$ is closely related to the density. The $Q\times f$ value for 0.4NZT-0.6CNT ceramics varies from 31200 GHz to 54400 GHz as the sintering temperature increases from 1325 °C to 1400 °C and a maximum $Q\times f$ value of 54400 GHz was obtained at 1375 °C. In addition, quality factor is also a function of materials composition. As shown in Fig. 7, the $Q\times f$ value decreases with increasing CNT content as expected because the $Q\times f$ value (17200 GHz) of CNT ceramics is much lower than that (170000 GHz) of NZT ceramics. The $Q\times f$ value of $(1-x)$NZT–xCNT ceramics sintered at 1375 °C decreases from 91730 GHz to 27150 GHz when the content of CNT increases from 0.2 to 0.8. Moreover, a considerably reduction in the $Q\times f$ value for 0.2NZT-0.8CNT ceramics was also observed according to the results in Fig. 7 and the maximum $Q\times f$ value is only 27150 GHz. It is reported that the $Q\times f$ value is influenced by many factors such as density, impurity, secondary phase and grain size as well as cation ordering [38]. As shown in Table 1, the densities of $(1-x)$NZT–xCNT ceramics with various x values are above 96%, the effect of density on the $Q\times f$ value can be neglected because the $Q\times f$ value is independent of relative density greater than 95% [39].The effects of impurity and secondary phase on the $Q\times f$ value might be neglected since the amount of Zn_2TiO_4 secondary phase is relatively few as shown in Fig. 2 and can not detected in the microstructures. Therefore, the decrease in the $Q\times f$ value should be related to the grain size and cation ordering. In general, a larger grain size means a smaller grain boundary, resulting in a reduction in lattice imperfection and then the $Q\times f$ value increases. As is discussed above, the

average grain size of (1-*x*)NZT-*x*CNT ceramics increases gradually with the increase of *x* value. However, the degree ordering of cation decreases steady with the increasing *x* value. As illustrated in Fig. 7, the $Q \times f$ value of 0.2NZT-0.8CNT ceramics is the lowest compared with the other compositions. Therefore, it seems that cation ordering is more crucial than grain size for a high quality factor in the solid solution between $A^{2+}B^{4+}O_3$ and $A^{3+}B^{3+}O_3$ complex perovskite compounds.

Fig. 8 shows the temperature coefficient of resonant frequency (τ_f) of (1−*x*)NZT–*x*CNT ceramics with different *x* values as a function of sintering temperature. In general, the temperature coefficient of resonant frequency is mainly governed by the composition, additive and secondary phase of a material. No significant change in the τ_f value for all the samples is observed when the composition remained unchanged ~~and no additive or secondary phase is detected~~ in the (1−*x*)NZT–*x*CNT ceramics, implying that the τ_f is almost independent of sintering temperature. It seems that a near-zero τ_f value can be achieved by adding CNT with a positive τ_f (+270 ppm/°C) to NZT with a negative τ_f (-42 ppm/°C). As expected, the measured τ_f value of (1−*x*)NZT–*x*CNT ceramics ranges from -36.4 to +55.9 ppm/°C with various CNT contents. At a sintering temperature of 1375 °C, a near-zero τ_f value of 0.3 ppm/°C was obtained for 0.4NZT-0.6CNT ceramics. In addition, an abrupt reduction in the τ_f value for *x* between 0.6 and 0.8 is also observed in Fig. 8, implying a phase transformation from the monoclinic structure with $P2_1/n$ space group to the orthorhombic structure with P*nma* space group. Similar behavior was found in $Nd(Mg_{1/2}Ti_{1/2})O_3$–$CaTiO_3$ and $Nd(Zn_{1/2}Ti_{1/2})O_3$–$CaTiO_3$ ceramic systems [16, 40]. But the detailed discussions have been not performed in these systems yet. In fact, cation ordering was suggested as a determining factor to affect the sign of τ_f in the investigation on the relationship between the

crystal structure and microwave dielectric properties of $La(Zn_{0.5}Ti_{0.5})O_3$ ceramics. As mentioned in Fig. 2, the cation ordering in NZT vanishes gradually with the increasing CNT amount. Therefore, it seems that the sharp variation for x from 0.6 to 0.8 in the τ_f of $(1-x)$NZT–xCNT system might be attributed to the elimination of cation ordering. The further investigation on structural characterization needs to perform by Rietveld crystal refinement and TEM techniques and is left for a future study.

4. Conclusions

The phase structure, microstructure and microwave dielectric properties of $(1-x)Nd(Zn_{0.5}Ti_{0.5})O_3$-$xCa_{0.61}Nd_{0.26}TiO_3$ ($0.2 \leq x \leq 0.8$) ceramics were extensively investigated as a function of $Ca_{0.61}Nd_{0.26}TiO_3$ content and sintering temperature. In all cases, the sintered ceramics showed the high relative densities and exhibited the double perovskite structure together with a small amount of Zn_2TiO_4 secondary phase. However, a phase transformation from monoclinic to orthorhombic structure was also observed when $x > 0.6$, accompanying with the disappearance of cation ordering. With an increase of $Ca_{0.61}Nd_{0.26}TiO_3$ content, dielectric constant (ε_r) increased due to the higher ε_r of CNT. And the quality factor ($Q\times f$) was depended to a large extent on the grain size and cation ordering of the ceramics. Moreover, it seemed that cation ordering was more crucial than grain size for a high quality factor of $(1-x)$NZT-xCNT ceramics. A near-zero temperature coefficient of resonant frequency (τ_f) could be obtained at $x = 0.6$ in the ceramics system. Furthermore, the sharp variation for x from 0.6 to 0.8 in the τ_f might be attributed to the elimination of cation ordering. Typically, excellent microwave dielectric properties of $\varepsilon_r = 56.3$, $Q\times f = 54400$ GHz and $\tau_f = +0.3$ ppm/^{o}C were obtained for $0.4Nd(Zn_{0.5}Ti_{0.5})O_3$-$0.6Ca_{0.61}Nd_{0.26}TiO_3$ sintered at 1375 ^{o}C for 4 h, suggesting that it could be used as a candidate

material for small-sized GPS patch antennas and 3G passive components.

Acknowledgements

This work was financially supported by Youth Foundation of Anhui University of Technology (Grant no.: QZ201307).

References

[1] I. Reaney, D. Iddles, Microwave dielectric ceramics for resonators and filters in mobile phone networks, J. Eur. Ceram. Soc. 89(2006) 2063–2072.

[2] M. Mirsaneh, O. Leisten, B. Zalinska, I. Reaney, Circularly polarized dielectric-loaded antennas: current technology and future challenges, Adv. Funct. Mater. 18(2008) 2293–2300.

[3] M. Sebastian, Dielectric Materials for Wireless Communication, Elsevier, 2008.

[4] W. Wersing, Microwave ceramics for resonators and filters, Curr. Opin. Solid State Mater. Sci. 1(1996) 715–731.

[5] B. Itaalit, M. Mouyanen, J. Bernard, J. Reboul, D. Houivet, Improvement of microwave dielectric properties of $Ba(Co_{0.7}Zn_{0.3})_{1/3}Nb_{2/3}O_3$ ceramics prepared by solid-state reaction, Ceram. Inter. 41(2015) 1937–1942.

[6] C. Ahn, H. Jang, S. Nahm, H. Park, H. Lee, Effects of microstructure on the microwave dielectric properties of $Ba(Co_{1/3}Nb_{2/3})O_3$ and $(1\text{-}x)Ba(Co_{1/3}Nb_{2/3})O_3\text{–}xBa(Zn_{1/3}Nb_{2/3})O_3$ ceramics, J. Eur. Ceram. Soc. 23(2003) 2473–2478.

[7] S. Cho, C. Kim, D. Kim, K. Hong, J. Kim, Dielectric properties of $Ln(Mg_{1/2}Ti_{1/2})O_3$ as substrates for high–T_c superconductor thin films, J. Mater. Res. 14(1999) 2484–2487.

[8] C. Tseng, C. Huang, W. Yang, C. Hsu, Dielectric characteristics of $Nd(Zn_{1/2}Ti_{1/2})O_3$ ceramics at microwave frequencies, J. Am. Ceram. Soc. 89(2006) 1465–1470.

[9] C. Hsu, Improved high-Q microwave dielectric resonator using ZnO-doped $La(Co_{1/2}Ti_{1/2})O_3$ ceramics, J. Alloys Compd. 464(2008) 412–417.

[10] C. Hsu, Y. Chang, Microwave characteristics of high-Q ZnO-doped $Nd(Co_{1/2}Ti_{1/2})O_3$ dielectric ceramics, J. Alloys Compd. 479(2009) 714–718.

[11] Y. Chen, K. Chang, S. Yao, Improved microwave dielectric properties of $Nd(Mg_{0.5}Sn_{0.5})O_3$ ceramics by substituting Mg^{2+} with Zn^{2+}, Ceram. Inter. 38(2012) 5377–5383.

[12]Y. Chen, Crystal structure and dielectric properties of $La(Mg_{1-x}Zn_x)_{1/2}Ti_{1/2}O_3$ ceramics at microwave frequencies, J. Alloys Compd. 509(2010) 1050–1053.

[13] C. Tseng, Substituting effects of Zn on microstructural characteristics and microwave dielectric properties of $Nd(Co_{1/2}Ti_{1/2})O_3$ ceramics, J. Am. Ceram. Soc. 91(2008) 4101–4104.

[14] J. Li, T. Qiu, Microwave dielectric properties of $Nd[(Zn_{1-x}Co_x)_{0.5}Ti_{0.5}]O_3$ ($0.025 \leq x \leq 0.1$) ceramics, Ceram. Inter. 38(2012) 2597–2600.

[15] C. Huang, C. Tseng, W. Yang, T. Yang, High-dielectric-constant and low-loss microwave dielectric in the $(1-x)Nd(Zn_{1/2}Ti_{1/2})O_3$–$xSrTiO_3$ system with a zero temperature coefficient of resonant frequency, J. Am. Ceram. Soc. 91(2008) 2201–2204.

[16] C. Tseng, C. Huang, W. Yang, Microwave dielectric properties of x $Nd(Zn_{1/2}Ti_{1/2})O_3$–$(1-x)CaTiO_3$ ceramics, Mater. Lett. 61(2007) 4054–4057

[17] M. Yoshida, N. Hara, T. Takada, A. Seki, Structure and dielectric properties of $Ca_{1-x}Nd_{2x/3}TiO_3$, Jpn. J. Appl. Phys. 36(1997) 6818–6823.

[18] C. Shen, C. Huang, C. Shih, C. Huang, The effect of $Ca_{0.61}Nd_{0.26}TiO_3$ addition on the microwave dielectric properties of $(Mg_{0.95}Ni_{0.05})TiO_3$ ceramics, J. Alloys Compd. 475(2009) 391–395.

[19] C. Huang, Y. Chien, C. Shih, H. Chang, Crystal structure and dielectric properties of xCa($Mg_{1/3}Nb_{2/3}$)O_3–(1-x)($Ca_{0.61}Nd_{0.26}$)TiO_3 at the microwave frequency, Mater. Res. Bull. 63(2015) 1–5.

[20] J. Qu, F. Liu, C. Yuan, X. Liu, G. Chen, Microwave dielectric properties of 0.2$SrTiO_3$-0.8$Ca_{0.61}Nd_{0.26}Ti_{1-x}Al_{4x/3}O_3$ ceramics, Mater. Sci. Eng. B 191(2015) 15–20.

[21] Q. Zhang, F. Wu, H. Yang, J. Li, Low-temperature synthesis and characterization of complex perovskite ($Ca_{0.61}$,$Nd_{0.26}$)TiO_3–($Nd_{0.55}$, $Li_{0.35}$)TiO_3 nanopowders and ceramics by sol–gel method, J. Alloys Compd. 508(2010) 610–615.

[22] B. Liang, X. Zheng, D. Tang, New high-ε and high-Q microwave dielectric ceramics: (1−x)$Ca_{0.61}Nd_{0.26}TiO_3$−xNd($Zn_{0.5}Ti_{0.5}$)O_3, J. Alloys Compd. 488(2009) 409–413.

[23] B. Hakki, P. Coleman, A dielectric resonator method of measuring inductive capacities in the millimeter range, IEEE Trans. Microwave Theory Tech. MTT-8(1960) 402–410.

[24] W. Courtney, Analysis and evaluation of a method of measuring the complex permittivity and permeability of microwave insulators, IEEE Trans Microwave Theory Tech MTT-18(1970) 476–485.

[25] M. Fu, X. Liu, X. Chen, Structure and microwave dielectric characteristics of $Ca_{1-x}Nd_{2x/3}TiO_3$ ceramics, J. Eur. Ceram. Soc. 28(2008) 585–590.

[26] H. Ohsato, H. Kato, M. Mizuta, S. Nishigaki, T. Okuda, Microwave dielectric properties of the Ba_{6-3x}(Sm_{1-y},R_y)$_{8+2x}Ti_{18}O_{54}$ (R=Nd and La) solid solutions with zero temperature coefficient of the resonant frequency, Jpn. J. Appl. Phys. 34(1995) 5413–5417.

[27] R. Shannon, Revised effective ionic radii and systematic studies of interatomic distances in halides and chalcogenides, Acta Cryst. A32(1976) 751–767.

[28] N. Setter, L. Cross, The role of B- site cation disorder in diffuse phase transition behavior of perovskite ferroelectrics, J. Appl. Phys. 51(1980) 4356–4360.

[29] H. Megaw, C. Darlington, Geometrical and structural relations in the rhombohedral perovskites, Acta Cryst. A3 (1975) 161–173.

[30] A. Glazer, The classification of tilted octahedral in perovskites, Acta Crystallogr. B28(1972) 3384–3392.

[31] A. Glazer, Simple ways of determining perovskite structures, Acta Crystallogr. A31(1975) 756–762.

[32] M. Seabra, A. Salak, V. Ferreira, J. Ribeiro, L. Vieir, Dielectric properties of (1-*x*)La($Mg_{1/2}Ti_{1/2}$)O_3–*x*$SrTiO_3$ ceramics, J. Eur. Ceram. Soc. 24(2004) 2995–3002.

[33] G. Babu, V. Subramanian, V. Murthy, Structure determination and microwave dielectric properties of La$(MgSn)_{0.5}O_3$ ceramics, J. Eur. Ceram. Soc. 27(2007) 2973–2976.

[34] S. Cho, H. Youn, H. Lee, K. Hong, Contribution of structure to temperature dependence of resonant frequency in the (1-*x*)La($Zn_{1/2}Ti_{1/2}$)O_3·*x*$ATiO_3$ (A = Ca, Sr) system, J. Am. Ceram. Soc. 84(2001) 753–758.

[35] I. Reaney, E. Collar, N. Setter, Dielectric and structure characteristics of Ba- and Sr-based complex perovskites as a function of tolerance factor, Jpn. J. Appl. Phys. 33(1994) 3984–3990.

[36] H. Tamura, T. Konoike, Y. Sakabe, K. Wakino, Improved high-Q dielectric resonator with complex perovskite structure, J. Am. Ceram. Soc. 67(1984) C59–C61.

[37] H. Matsumoto, H. Tamura, K. Wakino, Ba(Mg, Ta)O_3-$BaSnO_3$ high-Q dielectric resonator, Jpn. J. Appl. Phys. 30(1991) 2347–2349.

[38] W. Kim, E. Kim, K. Yoon, Effect of Sm^{3+} substitution on dielectric properties of

$Ca_{1-x}Sm_{2x/3}TiO_3$ ceramics at microwave frequencies, J. Am. Ceram. Soc. 82(1999) 2111–2115.

[39] D. Iddles, A. Bell, A. Moulson, Relationships between dopants, microstructure and the microwave dielectric properties of ZrO_2-TiO_2-SnO_2 ceramics, J. Mater. Sci. 27(1992) 6303–6310.

[40] C. Huang, Y. Chen, S. Lin, New dielectric material system of $Nd(Mg_{1/2}Ti_{1/2})O_3$– $CaTiO_3$ at microwave frequency, Solid-State Electron. 49(2005) 1921–1924.

Table captions

Table 1. Lattice parameter and density of (1-*x*)NZT-*x*CNT ceramics sintered at 1375 °C for 4 h.

Table 2. Approximate structure changes of (1-*x*)$Nd(Zn_{0.5}Ti_{0.5})O_3$-*x*$Ca_{0.61}Nd_{0.26}TiO_3$.

Figure captions

Fig. 1. Bulk density of (1-*x*)NZT-*x*CNT ceramics with different *x* values as a function of sintering temperature.

Fig. 2. X-ray diffraction patterns of (1-*x*)$Nd(Zn_{0.5}Ti_{0.5})O_3$-*x*$Ca_{0.61}Nd_{0.26}TiO_3$ ceramics with different *x* values sintered at 1375 ^{o}C for 4 h.

Fig. 3. 1/2(200) and 1/2(211) reflections of (1-*x*)$Nd(Zn_{0.5}Ti_{0.5})O_3$-*x*$Ca_{0.61}Nd_{0.26}TiO_3$ ceramics: (a) *x* = 0.2, (b) *x* = 0.4, (c) *x* = 0.6, (d) *x* = 0.8.

Fig. 4. SEM photographs of (1−*x*)NZT–*x*CNT ceramics sintered at 1375 °C for 4 h: (a) *x* = 0.2, (b) *x* = 0.4, (c) *x* = 0.6, (d) *x* = 0.8.

Fig. 5. SEM photographs of 0.4NZT–0.6CNT ceramics sintered at different temperatures for 4 h: (e) 1325 °C, (f) 1350 °C, (c) 1375 °C, (d) 1400 °C.

Fig. 6. Dielectric constant of (1−*x*)NZT–*x*CNT ceramics with different *x* values as a function of sintering temperature.

Fig. 7. $Q \times f$ value of $(1-x)$NZT–xCNT ceramics with different x values as a function of sintering temperature.

Fig. 8. Temperature coefficient of resonant frequency of $(1-x)$NZT–xCNT ceramics as a function of sintering temperature.

Table 1

x	Lattice parameter (Å)			Unit cell volume ($Å^3$)	X-ray density (g/cm^3)	Relative density (%)
	a	b	c			
0.2	5.47959	5.5778	7.78443	237.9	6.4532	97.11
0.4	5.46119	5.59736	7.76742	237.44	5.9561	99.44
0.6	5.45597	5.57153	7.80296	237.16	5.4239	98.14
0.8	5.45271	5.60041	7.75919	236.95	4.9309	98.76

Table 2

x	Tolerance factor	Cation ordering 1/2 (111)	Cation displacement 1/2 (210) 1/2 (300)	In-phase tilting 1/2 (321)	Anti-phase tilting 1/2 (311)	Space group
0.2	0.921	X	X	X	X	$P2_1/n$
0.4	0.93	X	X	X	X	$P2_1/n$
0.6	0.94	X	X	X	X	$P2_1/n$
0.8	0.949		X	X	X	P*nma*

[+] Based on XRD data only.

Fig. 1

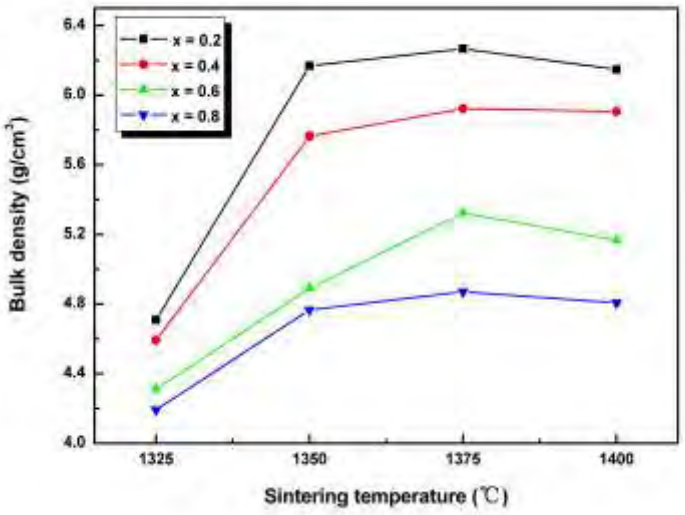

Fig. 2

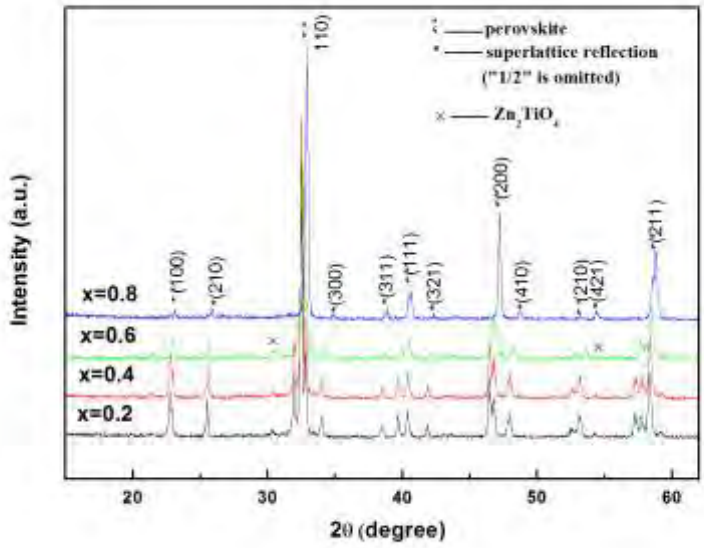

Fig. 3

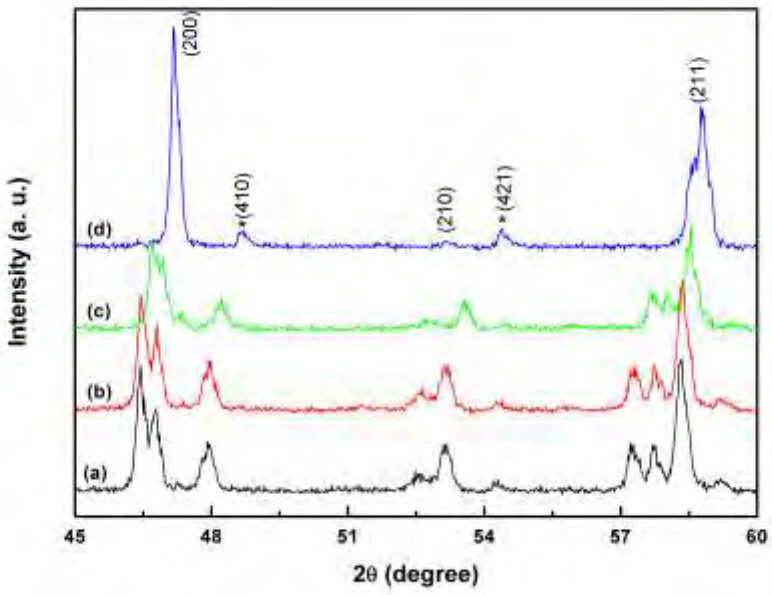

Fig. 4

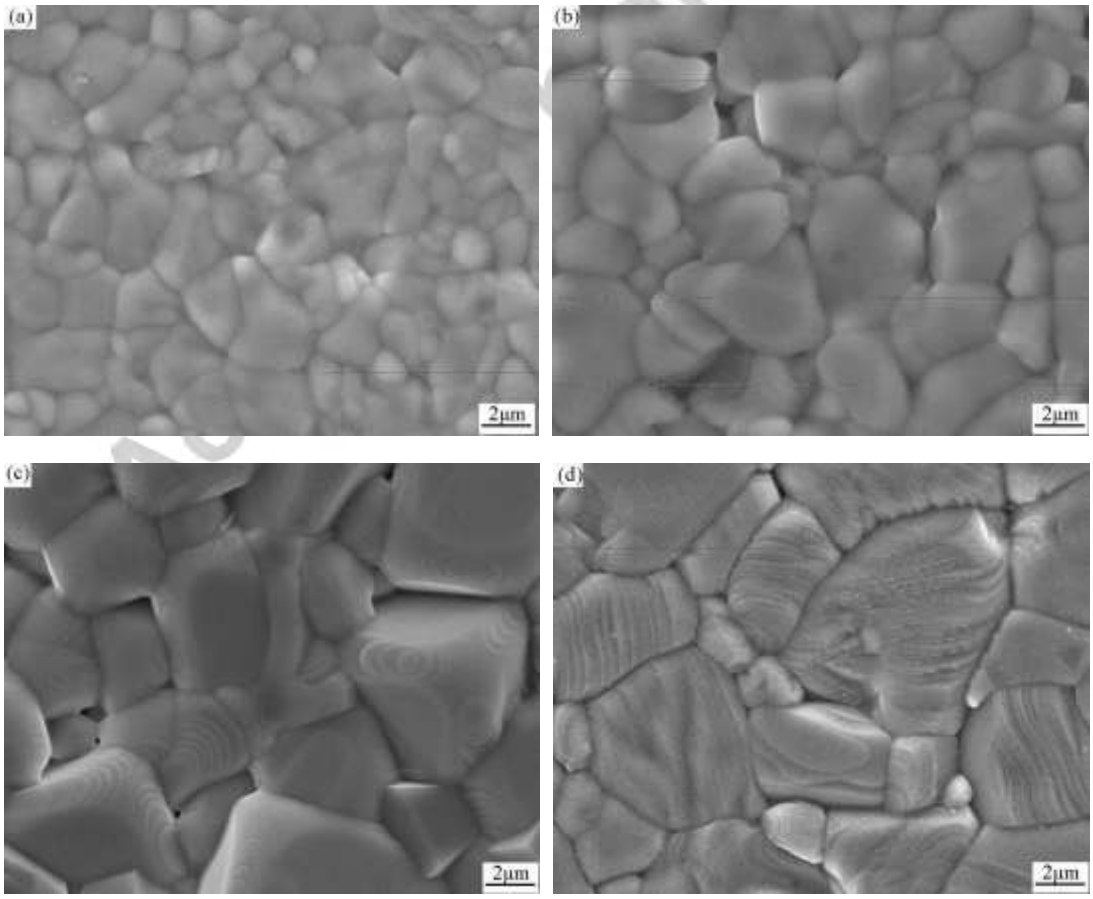

Fig. 5

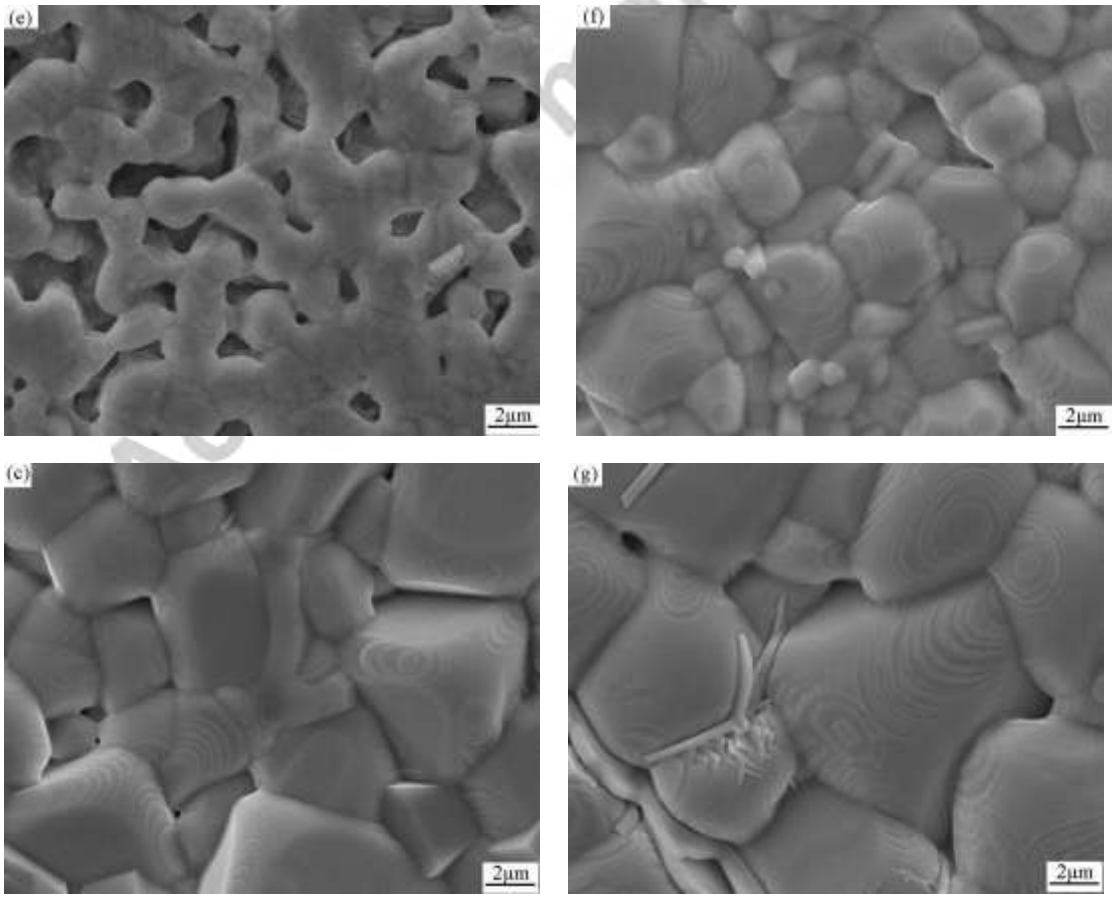

Fig. 6

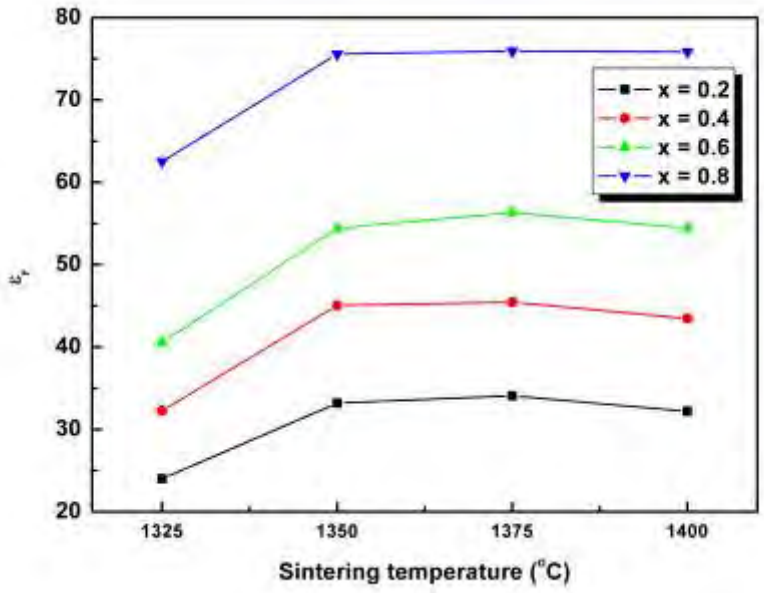

Fig. 7

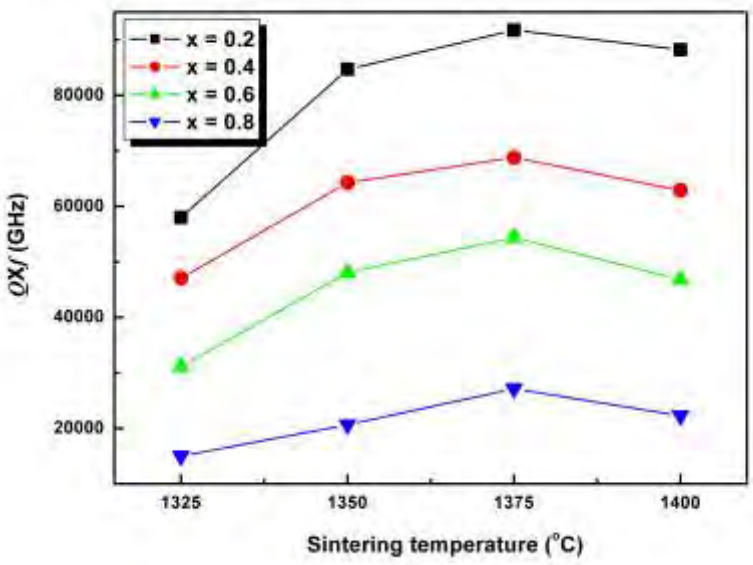
x = 0.2
x = 0.4
x = 0.6
x = 0.8
80000
60000
40000
20000
Qxf (GHz)
1325
1350
1375
1400
Sintering temperature (°C)

Fig. 8